Ocean Engineering 246 (2022) 110585

Contents lists available at ScienceDirect

Ocean Engineering

journal homepage: www.elsevier.com/locate/oceaneng

A flexible method for the initial prediction of tugs escort capability

Francesco Mauro

University of Strathclyde, Maritime Safety Research Centre (MSRC), Department of Naval Architecture Ocean & Marine Engineering, 100 Montrose Street, Glasgow G40LZ, UK

ARTICLE INFO

Keywords:
Escort tug
Thrust allocation
Stability
Performance predictions

ABSTRACT

Preliminary prediction of escort tug capability aims to identify the maximum steering and braking forces the tug could deliver during operations at sea. To this end, the adoption of a steady-state equilibrium approximation ensures attaining a quick and enough accurate results for the initial design stage. Diverse techniques are suitable to resolve the equilibrium, with different simplification levels and related limitations. In this study, a method based on a nonlinear thrust allocation algorithm is improved, including propulsors interactions. Moreover, the addition of the transversal equilibrium modelling of the tug allows evaluating the compliancy with stability and safety Regulations for escort class. The coupling between enhanced equilibrium resolution and a simplified approach to estimate the hydrodynamic forces results in a flexible prediction method for tug escort capability, which is requiring few inputs, without excluding the possibility to use higher fidelity hydrodynamic loads. The calculation framework, implemented with different levels of confidence for hydrodynamic loads, is tested on different tug types, highlighting its flexibility compared to more traditional and widely accepted approaches for the initial design stage.

1. Introduction

The necessity to reduce the risk of accidents for large merchant ships while approaching harbours or navigating in restricted waters implies the assistance of dedicated vessels (Iglesias-Baniela et al., 2021; Paulauskas et al., 2021; ETA, 2015). These units, named escort tugs, are specifically designed to produce a sufficiently large amount of steering and braking forces necessary to control the escorted ship. Conventional tugs generate braking force by using the propulsive devices mounted onboard (Sas et al., 1993). Thus, conventional tugs performances are strictly related to the amount of power installed. However, propulsion is not the unique way to generate force for an escort tug, as, with a drift angle, the interaction between hull and fluid could potentially produce a larger force amount (Allan and Molyneux, 2004). For such a reason, the escort tug is dealing with both propulsive and hydrodynamic forces, transmitting them to the escorted ship through the towing line. Therefore, the tug is subject to three different time-varying force sources, dependent upon mutual position and speed between the tug and escorted ship. A detailed simulation of such phenomenon requires the numerical reproduction of a complete escort operation (Piaggio et al., 2019), thus the knowledge of project details not available in an early design stage. For a preliminary calculation the problem can be reduced to a static approximation (Quadvlieg and Kaul, 2006; Bucci and Marinò, 2016), solving the equilibrium of the steady-state forces according to different boundary conditions, identifying the maximum steering and braking forces the tug could deliver.

Different methods allow solving the steady-state equilibrium, having diverse levels of approximation. It is common practice to adopt very simplistic approaches (Allan and Molyneux, 2004; Bucci et al., 2016; Tackinaci and Erginer, 2017; Aydin et al., 2018; Yastreba, 2018), grouping all the propulsive devices in a single equivalent unit and imposing simplifications on the total thrust orientation. However, the adoption of more advanced techniques, derived from traditional dynamic positioning thrust allocation solvers, improves the ability to identify preliminary escort performances of the tug (Mauro, 2021). In any case, all the mentioned processes do not take into account limitations due to tug stability. Harmonised regulations in charge from January 2020 and amended to the Part B of the International code on intact stability 2008 (IMO, 2016) impose safety limits on the tug heeling during escort operations (Allan, 2006; de Jong, 2007). The presence of these limitations could influence the maximum steering and braking forces an escort tug could deliver. To this end, the reformulation of a methodology based on the thrust allocation algorithm allows handling such safety constraints. Furthermore, being the macro-category of escort tugs constituted by several unit types (Hyslop et al., 2018), the method should accomplish different tug typologies, including ASD tugs, tractor tugs and rotor tugs.

The enhanced methodology for the equilibrium determination (METHOD 1) has been applied to a set of escort tugs of different typologies to provide a flexible framework for initial escort capability prediction. The process can be applied with different levels of

E-mail address: francesco.mauro@strath.ac.uk.

https://doi.org/10.1016/j.oceaneng.2022.110585
Received 20 July 2021; Received in revised form 30 November 2021; Accepted 6 January 2022
Available online 29 January 2022
0029-8018/© 2022 The Author. Published by Elsevier Ltd. This is an open access article under the CC BY license (http://creativecommons.org/licenses/by/4.0/).

Nomenclature

β	Drift angle
β_p	Propeller hydrodynamic pitch
Δ	Vessel displacement
δ	Propeller inflow angle
γ	Towing force angle in the tug reference system
$\overline{GM}_T$	Transversal metacentric height
$\overline{GZ}$	Righting lever curve
ϕ	Heeling angle
ρ	Water density
τ	Towing force angle in the escorted ship reference system
ξ	Interaction factor
C_B	Block coefficient
C_T	Propeller thrust coefficient
C_x, C_y, C_M	Hydrodynamic forces/moment coefficients
C_X	Dynamic propeller characteristics in cross-flow in x direction
D	Propeller diameter
D_H	Hydrodynamic drag
F_B	Braking force
F_H	Hydrodynamic force
F_P	Propulsor force
F_S	Steering force
F_T	Towing force
F_x	Longitudinal force component
F_y	Lateral force component
F_{Pmax}	Maximum propulsor force
g	Gravity acceleration
L_H	Hydrodynamic lift
L_{PP}	Length between perpendiculars
M_x	Heeling moment
M_z	Yaw moment
N_P	Number of propulsors
T	Tug draught
V_A	Propeller advance speed
V_r	Propeller relative speed
V_S	Vessel escort speed
x_P	Longitudinal position of the propulsor
x_T	Longitudinal position of the towing force application point
y_P	Lateral position of the propulsor
y_T	Lateral position of the towing force application point
z_P	Vertical position of the propulsor
z_T	Vertical position of the towing force application point

approximation, depending on the evaluation of hydrodynamic forces; e.g., using a simplified state of art procedure (LEVEL 1), or, if available, using CFD or model test experiments on similar units (LEVEL 2). This approach allows a general scheme for preliminary escort capability determination that needs few inputs, as requested during an initial design stage. The application of this framework on the test tugs shows advantages compared to traditional methods (METHOD 0), using both simplified or higher fidelity hydrodynamic loads. The adoption of different fidelity levels for the hydrodynamic forces leads to differences from 5 to 30% in the maximum forces delivered in safe working conditions, depending on the tug type. These differences are acceptable for a preliminary design stage prediction but stress out the necessity to develop empirical hydrodynamic forces models specific for escort tugs. Finally, the analysis highlights the importance to include safety criteria, besides already introduced propulsor modelling, since initial calculations.

2. Escort tug characteristics

An escort tug is a unit designed to fulfil specific assistance duties to large ships approaching harbours or sailing in restricted waters. Therefore it should be capable of delivering sufficiently high steering and braking forces to control the speed and motions of the escorted ship. These forces change with the speed, the towing angle inclination and the drift angle of the tug; however, in an initial design phase, it is advisable to evaluate the maximal performances of the unit.

In an initial design phase, the determination of the global escort characteristics of a tug is solved with a quasi-steady approach to reduce the calculation time and the amount of input needed. The standard process consists of solving the global equilibrium of forces acting on the tug in the horizontal plane, described by the following set of equations in a tug-fixed reference system (see Fig. 1):

$$F_{T_x} + F_{P_x} = F_{H_x} \tag{1}$$

$$F_{T_y} + F_{P_y} = F_{H_y} \tag{2}$$

$$M_{T_z} + M_{P_z} = M_{H_z} \tag{3}$$

In the formulas, the subscript T indicates towing line actions, P propulsive actions and H hydrodynamic ones in x, y and z directions. Several procedures allow the resolution of the equilibrium. The most simple ones consider the propulsors grouped in a single equivalent unit, whilst more advanced methods could handle each thruster individually through an optimised allocation algorithm. However, escort operations modalities depend on the escort tug type employed for the service.

2.1. Escort tug types

Efficient escort performances result from tugs having excellent manoeuvre capability, high propulsive thrust, and large steering and braking forces aft of the assisted ship. In general, these characteristics are achievable by adopting a propulsion system potentially locating maximum thrust around 360 degrees. Vertical axis rotors or azimuthal thrusters give the required flexibility. However, the propulsive system can be installed in different positions along the hull, requiring specific hull forms for the installation. That is leading to different kind of tugs and escort modes. For such a reason, it is necessary to distinguish between the main typologies of escort tug populating the worldwide tug fleet.

2.1.1. Stern drive (ASD) tugs

This category of tug is probably the most commonly adopted in the world. The propulsive configuration of the vessel is composed of two azimuth thrusters located at the vessel stern. This configuration gives the possibility to have sufficiently high manoeuvrability while keeping high the achievable bollard pull value. ASD tugs are not used only for escort operations but also for standard towings. The towing winch is placed at the bow, performing the escort operation with the tug oriented as reported in Fig. 1(a).

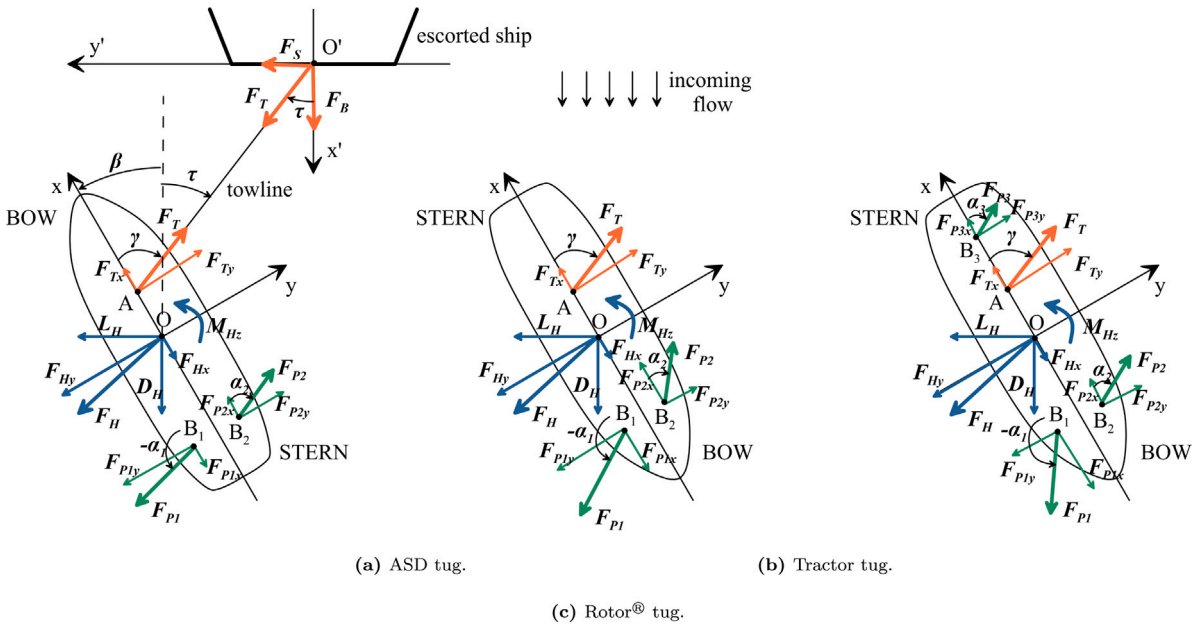

(a) ASD tug. (b) Tractor tug.

(c) Rotor® tug.

Fig. 1. Reference system and forces scheme for different escort tug types.

2.1.2. Tractor tugs

The tractor tug (or originally water tractor) is an escort tug concept initially developed to install cycloidal propellers as a propulsive device. Nowadays, the tractor units adopt also azimuth thrusters for steering and propulsion. In both cases, the propulsion/steering system is located in one of the vessel ends (generally to the bow) at the hull bottom and is composed of two devices installed at the same longitudinal position, so being shifted only in the lateral direction. Special protections installed around or in front of the propulsive device shield the propulsors from contacts or groundings. The resulting hull shape generally grants higher maneuvring characteristics compared to a conventional ASD tug. However, it is necessary to fit an additional fin on the opposite end of the vessel to propulsors' position to balance the steering and braking forces. Tractor tugs perform the escort operations by the stern, following the tug orientation as in Fig. 1(b).

2.1.3. Rotor tugs

This particular escort tug is a patented concept in the tug design with a unique propulsion system utilising three main engines, each driving an azimuth propulsion unit. Two propulsion units are located forward off the centreline, in the standard tractor configuration, with the third unit aft off the centreline replacing the traditional aft skeg. The lack of a substantial skeg reduces resistance to turning and cuts down the influence of a ship propeller wash when working close to large vessels underway. For rotor tugs, it is also possible to perform the escort activities by the bow or by the stern, Fig. 1(c) shows the second possibility.

2.2. Stability requirements

Besides the necessity to develop sufficiently high steering and braking forces, it is crucial to operating with an appropriate safety level. When a tug is escorting a vessel with a certain speed, the instantaneous forces acting on the unit generate a heeling moment. Therefore, it is necessary to check whether the tug has a sufficient reserve of stability in these operative situations.

For this purpose, the classification societies have issued some particular requirements for escort tug stability. The guidelines account for combinations of environmental conditions and operation profiles, properly defining a set of tailored service notations. However, multiple classification societies have set different standards for escort notations, but after a dedicated JIP (de Jong, 2007), IMO adopted specific amendments in the Intact Stability code (IMO, 2016), providing harmonised rules effective from January 2020.

The harmonised rules apply the following criteria, taking as key stability issue the residual area under righting lever curve:

$$\begin{cases} A \geq 1.25B \\ C \geq 1.40D \\ f > 0 \end{cases} \tag{4}$$

where A is the area under the righting lever curve and B is the area under the heeling lever curve, both measured from the static equilibrium angle ϕ_c up to 20°. C and D are also areas under righting and heeling lever but evaluated between 0° and ϕ_d, being ϕ_d the minimum between downflooding angle and 40°. Fig. 2 shows an overview of these two criteria. The third constraint refers to the freebord f, which should be positive for all the possible operating profiles.

The dynamic stability criteria imply constraints on the maximum heeling angle the tug can have with a sufficient safety level. Consequently, this limitation reflects also on the maximum transversal force the tug can generate; thus on the escort performances of the vessel.

2.3. Reference tugs

Through this study three reference tugs are analysed, representative of the three categories described in the previous sections. *TUG#1* is a sample tractor tug, used by the author in a previous study (Mauro, 2021). This unit is used as reference for the enhancements applied to the capability assessment method. *TUG#2* is an example of ASD tug, *TUG#3* is an example of rotor tug. Table 1 reports a resume of the main characteristics of the three units considered in this study.

For *TUG#1*, hydrodynamic forces derive from CFD calculations available in literature (Smoker, 2012). For *TUG#2* experimental results and CFD calculations are available for a unit of equivalent size (Piaggio et al., 2020). The last tug has been also analysed with CFD, using the same mesh an calculation settings as suggested by the validation study presented in Smoker et al. (2016a). The previous studies report generally good agreement between numerical simulations and model tests, with differences related mainly to the exact detection of stall angle. However, the values are always within 30% of the experimental values. Further considerations on hydrodynamic forces are presented

Table 1
Reference tugs main characteristics.

	Symbol	*TUG#1*	*TUG#2*	*TUG#3*	Unit
Length between perpendiculars	L_{PP}	33.0	25.0	36.0	m
Length overall	L_{OA}	35.0	27.5	39.0	m
Maximum breadth	B	12.1	10.0	14.0	m
Design draught	T	4.0	3.6	4.1	m
Displacement (salt water)	Δ	1023.4	542.7	1315.1	t
Transversal metacentric height	$\overline{GM}_T$	1.95	2.25	2.32	m
Number of propulsors	N_P	2	2	3	–
Maximum propulsor force	$F_{P_{max}}$	2 × 175.5	2 × 225.4	3 × 279.5	kN

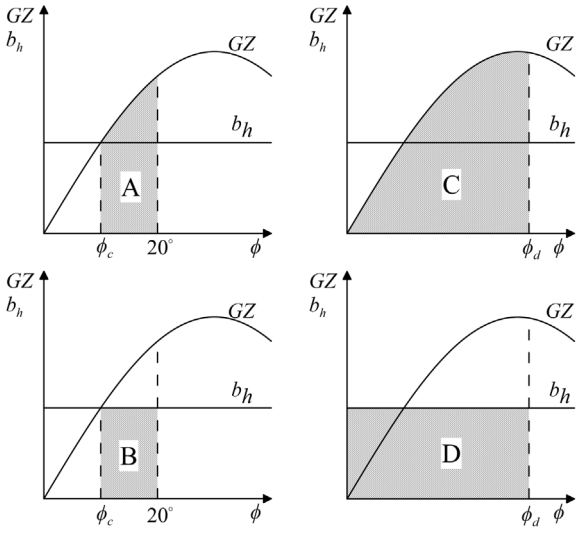

Fig. 2. Reference areas for escort operations dynamic stability criteria.

and discussed in a dedicated session, comparing CFD results with simplified models.

Fig. 3 shows a short overview of the layouts and the profiles of the tugs used in this study. For *TUG#3* also the alternative towing point A' is reported; however, all analyses refer to point A for the application of towing force.

3. Enhanced equilibrium resolution

Regardless the tug types, the same techniques applies to the equilibrium resolution. Most of the methods available in literature consider the grouping of all the thrusters into a single equivalent unit. However, as this assumption can be too simplistic especially when more than two thruster units are present, this work adopts a more advanced method based on thrust allocation algorithm.

The target for thrust allocation is the minimisation of absorbed power, that is expressed as a function of the delivered thrust, resulting in the following objective function:

$$\min(z) = \sum_{i=1}^{N_P} \left(F_{P_{xi}}^2 + F_{P_{yi}}^2 \right)^{1/3} \tag{5}$$

where N_P is the number of propulsors installed on the tug. The optimisation process for the equilibrium resolution requires the definition of a set of constraints. A first set derives from Eqs. (1), (2) and (3), with the following formulations:

$$F_{T_x} + \sum_{i=1}^{N_P} F_{P_{xi}} = F_{H_x} \tag{6}$$

$$F_{T_y} + \sum_{i=1}^{N_P} F_{P_{xi}} = F_{H_y} \tag{7}$$

$$-F_{T_x} y_T + F_{T_y} + \sum_{i=1}^{N_P} \left(-F_{P_{xi}} y_{Pi} + F_{P_{yi}} x_{Pi} \right) = M_{H_z} \tag{8}$$

where x_T, y_T and x_{Pi}, y_{Pi} are the longitudinal and lateral position of the towline application point and propulsor devices respectively. Besides these equations representative of the static equilibrium of the tug, additional constraints should identify the maximum thrust limits for each propulsor. In this study, the maximum thrust constraints refer to the cross-flow modelling described in Mauro (2021), where the propulsor is modelled with a Ka 4–70 propeller working in 4 quadrants. The propeller thrust coefficient is as follows:

$$C_T = \frac{8}{\pi} \frac{\sqrt{F_{P_x}^2 + F_{P_y}^2}}{\rho V_r^2 D} \tag{9}$$

where D is the propeller diameter and V_r is the relative speed at $0.7D$. The thrust components change according to the inflow speed, more precisely with the advance angle β_p, and with the inflow angle δ between thruster orientation and flow direction. Fig. 4 shows the effect of β_p and δ on C_T, together with the linearisation of the envelope. A detailed description of the constraints generation is given in Mauro (2021).

The conventional methods adopted to evaluate the equilibrium on escort tugs are not considering the propulsors individually. The following simplified procedures are widely used to predict tug escort performances:

- *Pure indirect method*: the delivered propulsor thrust is always oriented in the tug y direction. Therefore, the F_{P_x} component in Eq. (1) is equal to zero, and the lateral propulsor force F_{P_y} is directly derived from Eq. (2). The process is repeated for a set of β angles, obtaining the towline force F_T and the towline angle τ.
- *Powered indirect method*: this method derives from the previous one, deriving the lateral propulsor force from Eq. (2). The longitudinal component F_{P_x} of Eq. (1) is determined by imposing the usage of all the available thrust onboard:

$$F_{P_x} = \sqrt{F_{Pmax}^2 - F_{P_y}^2} \tag{10}$$

  This identity is valid only for $F_{P_y} < F_{Pmax}$, allowing the determination of F_T and the towline angle τ on a predefined β range.
- *Iterative method*: this method is not assuming additional constraints on the propulsor force. To this end, the number of dependent variables is reduced by considering β, τ and F_T as dependent variables. However, the resolution of Eqs. (1) and (2) does not ensure the moment balancing of Eq. (3). The moment is solved searching the equilibrium for a fixed range of F_T at each combination of τ and β, allowing the determination of the maximum towing force for each angles.

Compared to simplified procedures, the advanced propulsor modelling and the equilibrium resolution via thrust allocation algorithm allow predicting a broader range of feasible equilibrium solutions. The method also detects higher maximum steering and braking forces. As an example, Fig. 5 shows a comparison of the capability results obtained

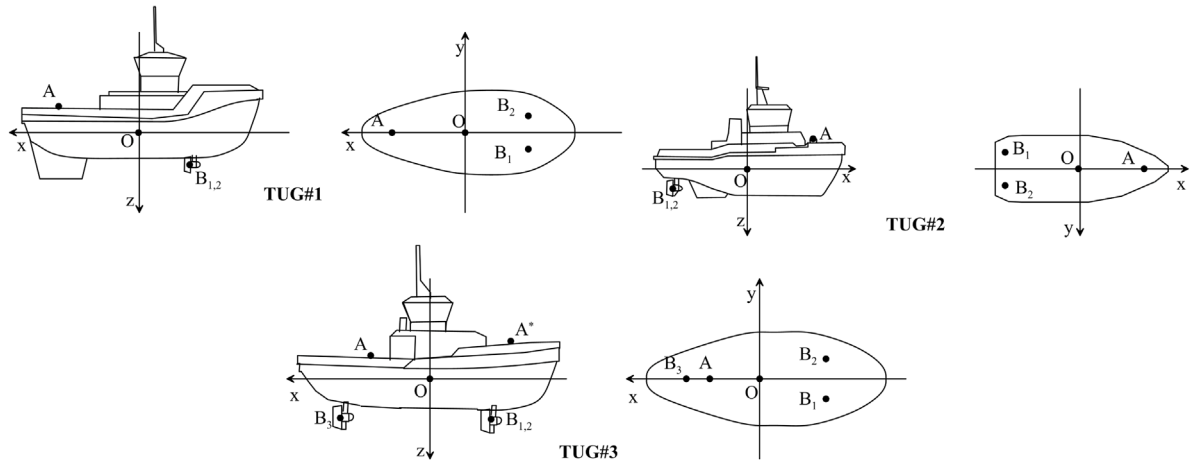

Fig. 3. Overview of the reference escort tugs.

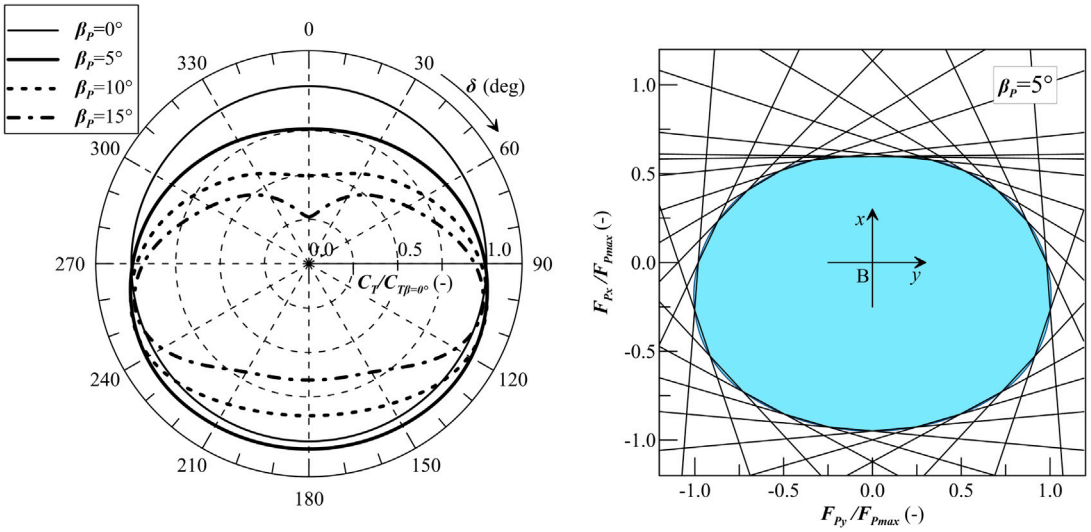

Fig. 4. Thrust coefficient at different β_p (*left*) and thrust envelope reproduction with linear constraints for $\beta_p = 5°$ (*right*).

applying the propulsor modelling method and simplified methods for the *TUG#1*.

Even though the advanced propeller modelling provides the stated advantages, some weaknesses are still there. In the present form, the procedure does not include the interaction effect between propulsors and also the possible shield effect given by the presence of a skeg. Moreover, there are no limitations to the maximum heeling moment necessary for compliance with regulations. These two aspects are worthy of investigation to enhance the resolution method, aiming at a flexible procedure for initial predictions.

3.1. Transversal equilibrium

A relevant issue for the global capability of escort tugs is to verify stability during operations. As highlighted in the previous sections, classification societies impose limitations to the maximum safe heeling angle according to dynamic stability criteria. Therefore, to evaluate the compliance of the tug working conditions with such stability requirements, the transversal rotation equilibrium of the vessel along x axis needs to be analysed. The following equation describes the tug's stability and is complementary to the equilibrium system:

$$-F_{T_y} z_T - \sum_{i=1}^{N_P} F_{P_{yi}} z_{P_i} - F_{H_y} z_H = M_R(\phi) \tag{11}$$

where z_T, z_{P_i} and z_H are the vertical positions of the towline application point, propulsor thrust and hydrodynamic force, respectively. M_R is the righting moment of the vessel, changing as a function of heeling ϕ. M_R is given by $\Delta\overline{GZ}(\phi)$, where Δ is the tug displacement and $\overline{GZ}(\phi)$ is the righting lever curve. As the $\overline{GZ}$ has a non-linear behaviour, its expression could be even more simplified, adopting, for example, the metacentric approximation. This is more convenient in an initial design stage, when the hull form necessary to determine $\overline{GZ}$ curve is not definitive or available. In such a case, the heeling angle at the equilibrium became directly determinable by the following equation:

$$\phi = \arcsin \frac{-F_{T_y} z_T - \sum_{i=1}^{N_P} F_{P_{yi}} z_{P_i} - F_{H_y} z_H}{g\Delta\overline{GM}_T} \tag{12}$$

where $\overline{GM}_T$ is the transversal metacentric height. In case the effective $\overline{GZ}$ curve is available, the equilibrium heeling can be found by interpolation or successive approximations.

By knowing the heeling angle at each equilibrium position, it is then possible to determine the compliance with stability criteria described in (4). Testing these criteria for *TUG#1* allows detecting the impact of a safe heeling on the global escort characteristics. Moreover, the same case permits comparing the results of the metacentric approximation and the $\overline{GZ}$ curve for the transversal rotation. Fig. 6 shows the obtained results in polar form for the towing speeds of 6, 8 and 10 knots. The criteria limits used for the analysis are as follows:

Table 2
Escort performances of *TUG#1* with heeling constraints using $\overline{GZ}$ curve and metacentric approximation.

V_s	Quantity		1 criterium exceeded		1+2 criteria exceeded		No criteria	
			GZ	Metacentric	GZ	Metacentric	GZ	Metacentric
6.0 kn	Maximum towline force	$F_{T_{max}}$	650.0	650.0	650.0	650.0	650.0	650.0
	Maximum braking force	$F_{B_{max}}$	550.0	550.0	550.0	550.0	550.0	550.0
	Maximum steering force	$F_{S_{max}}$	634.6	634.6	634.6	634.6	634.6	634.6
8.0 kn	Maximum towline force	$F_{T_{max}}$	727.2	727.2	1045.0	1053.3	1053.3	1053.3
	Maximum braking force	$F_{B_{max}}$	187.5	187.5	920.0	920.0	920.0	920.0
	Maximum steering force	$F_{S_{max}}$	688.3	688.3	937.2	945.6	945.6	945.6
10.0 kn	Maximum towline force	$F_{T_{max}}$	735.0	740.0	1115.0	1115.0	1600.0	1600.0
	Maximum braking force	$F_{B_{max}}$	195.0	195.0	195.0	195.0	1380.0	1380.0
	Maximum steering force	$F_{S_{max}}$	666.1	670.6	1077.0	1077.0	1332.6	1332.6

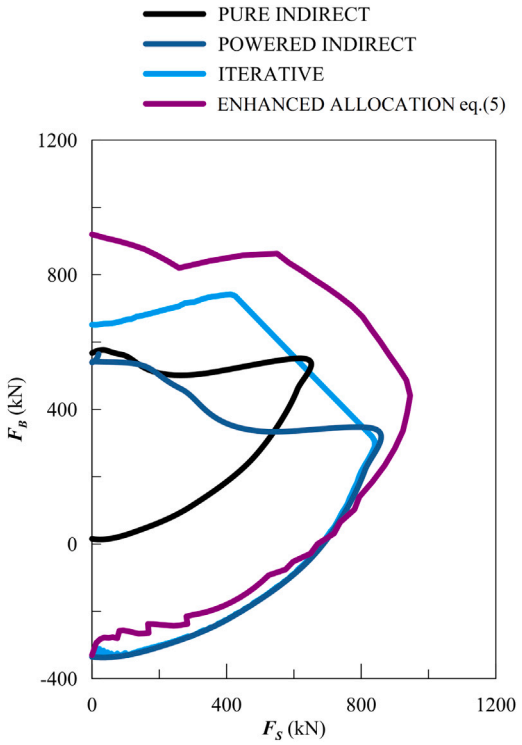

Fig. 5. Cartesian representation of the escort performances for *TUG#1* at the speed of 8 knots using different resolution methods (Mauro, 2021).

- *Criterium 1*: is the minimum heeling angle between the dynamic stability criteria described in (4). The values between the two criteria are close to each other, therefore, for a simpler representation the minimum between the two has been selected. The value for *TUG#1* using the $\overline{GZ}$ curve is 12.6°, while it changes to 13.2° applying the metacentric approximation. It has to be observed that the obtained values are inside the validity of the metacentric approximation.
- *Criterium 2*: is the heeling angle associated to the condition $f = 0$, corresponding to 20.5° for *TUG#1*.

Table 2 contains the results of the analysis. For the speed of 6 knots, the operations are always safe for the considered tug, thus the criteria does not change the potential performances. However for the higher speeds, the situation changes and criteria play an important role for the potential escort performances.

Analysing the graphs and tables it is possible observing that the metacentric approximation provides almost the same envelops for the towing force at all the tested speeds, having a difference of less than 1% on the predicted forces values. Thus, the metacentric approximation can be an acceptable solution for tugs in an initial design stage.

3.2. Interaction effects

The use of azimuthal thrusters onboard tugs implies that the devices are installed close to each other, thus reciprocally influencing the propulsive performances. Once the wake of a thruster washes the other unit, the inflow to the propeller is disturbed. Consequently, the dynamic properties of the second thruster change, decreasing the maximum available thrust. This effect has been studied by several authors (Lehn, 1980; Brandner and Renilson, 1998), providing possible ways to model the interaction effect. In offshore applications for dynamic positioning, it is common practice for capability calculations to consider forbidden zones between thrusters to avoid interaction problems, or adopt alternative thrust allocation strategies to consider interaction effects (Arditti et al., 2019; Prpić-Oršić and Valčić, 2020; Mauro and Nabergoj, 2016). However, in a tug, the thruster control is manual, not automatic, so the forbidden areas are not applicable. Consequently, the master cannot easily avoid thruster–thruster interaction, and the thrust allocation algorithm should consider it for predictions.

A possible approach is to consider the interaction modelling according to Brandner and Renilson proposal (Brandner and Renilson, 1998). The method supposes that the front thruster operates in open-water conditions; the thrusters behind it work in its wake, suffering for interaction effect depending on their reciprocal position. When the second thruster wholly operates in the foremost thruster wake, it operates in the so-called full-interaction condition, with the following advance angle for the propeller corresponding to an equivalent advance angle of the wake race:

$$\beta_{p_R} = \frac{1}{2}\left[\tan\beta_{pv}\,(2\cos\delta - 1) + \sqrt{\tan\beta_{pv}\,(2\cos\delta - 1)^2 + \frac{2kC_X}{\cos^2\beta_{pv}}}\right] \tag{13}$$

where β_{pv} is the virtual advance angle (thus without including wake fraction for the inflow speed), C_X is the propeller thrust coefficient in x direction and k is a constant equal to 0.43 but can be adjusted if experimental data are available.

The process allows determining the dynamic characteristics of the thruster acting in full-interaction condition. However, the portion of the propeller disk area influenced by the wake changes due to the different possible thruster orientations. Adopting a cylindrical model for the thruster wake as outlined in Abramovich (1960) permits the description of the race trajectory evaluating the interaction factor between the two thrusters:

$$\xi = \frac{1}{2\pi}\left[(\lambda_D - \sin\lambda_D) + \left(\frac{D_R}{D_D}\right)^2(\lambda_R - \sin\lambda_R)\right] \tag{14}$$

The quantities λ_D and λ_R are a function of the mutual positions of the propeller disks, propeller diameters and wake race diameter D_R. From the interaction factor ξ, it is possible to determine the forces in x and y directions delivered from the thruster in disturbed flow:

$$F_{P_x} = \xi\left(F_{P_x}(\beta_p,\delta)_R - F_{P_x}(\beta_p,\delta)_O\right) + F_{P_x}(\beta_p,\delta)_O \tag{15}$$

$$F_{P_y} = \xi\left(F_{P_y}(\beta_p,\delta)_R - F_{P_y}(\beta_p,\delta)_O\right) + F_{P_y}(\beta_p,\delta)_O \tag{16}$$

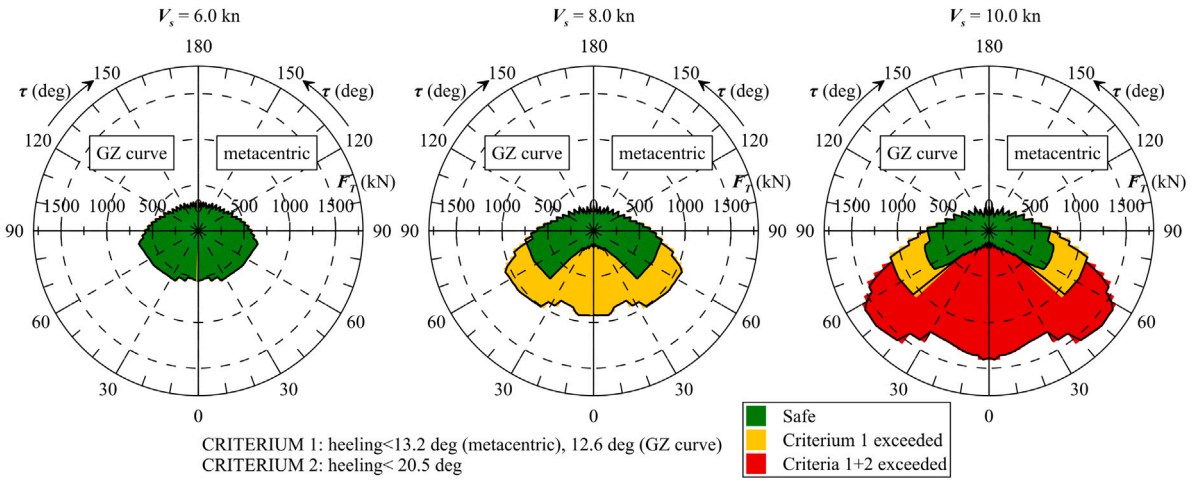

Fig. 6. Effect of stability criteria on *TUG#1* escort operability at different speeds, considering $\overline{GZ}$ curve and metacentric approximation.

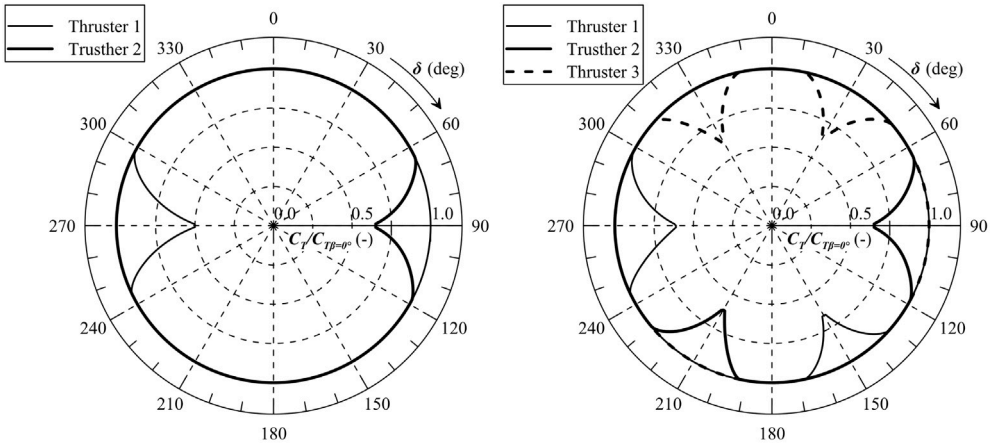

(a) Interaction between two thrusters. **(b)** Interaction between three thrusters.

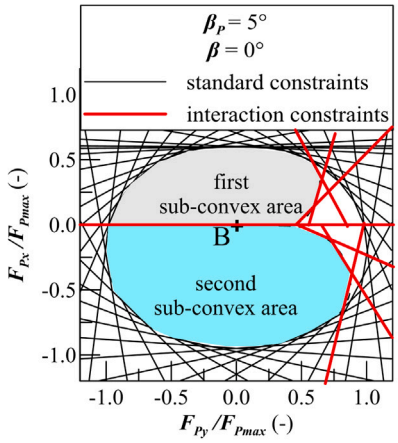

(c) Constraint linearisation.

Fig. 7. Effect of thruster–thruster interaction on propeller C_T for $\beta_p = 0°$ and constraint linearisation example for $\beta_p = 5°$.

So the method uses only the forces of the open-water condition $F_P(\beta_p, \delta)_O$ and the full-interaction one $F_P(\beta_p, \delta)_R$ to determine the final thrust. Fig. 7(a) shows an example of the interaction between two thrusters for $\beta_p = 0°$ determined by applying the above-described procedure.

The method can be extended to the three thrusters case, also covering the instance of Rotor tugs. Fig. 7(b) gives an example of the interaction procedure with three thrusters for $\beta_p = 0°$.

The interaction envelope can be also linearised as for the propeller modelling. However, the interaction modelling generates a convex

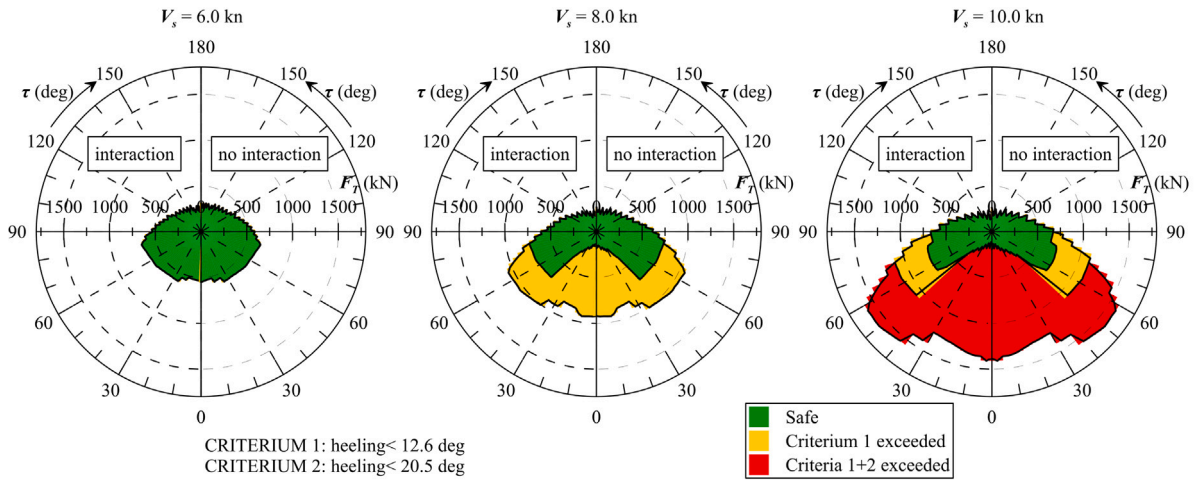

Fig. 8. Effect of interaction modelling on *TUG#1* escort capabilities at different speeds.

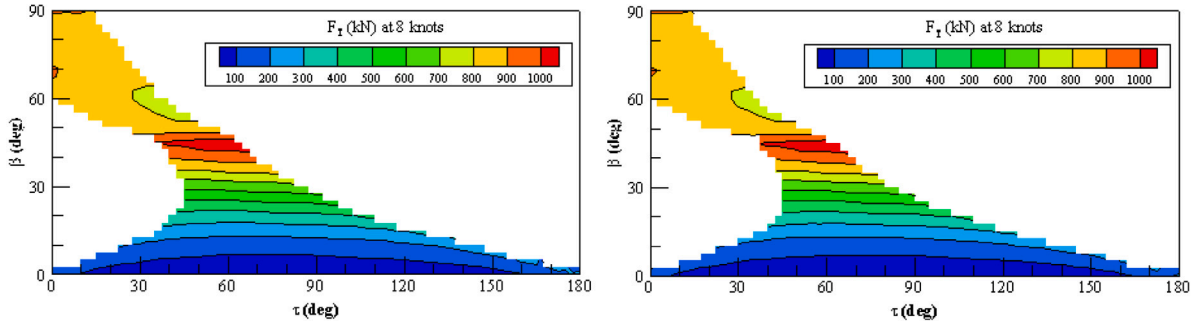

Fig. 9. Towing force contour plot without (*left*) and with (*right*) thruster interaction for *TUG#1* at the speed of 8 knots.

envelope for each thruster, regardless for the advance speed. To solve this problem, an iterative process during the optimisation, activating proper convex sub-regions according to the variables values, as performed with high β_p's (Mauro, 2021). Fig. 7(c) shows an example of the convex sub-regions for the case of $\beta_p = 5°$.

The application of the interaction procedure on *TUG#1* indicates that the disturbed flow has not a huge impact on the escort capability of the vessel. The maximum towing forces remain comparable with the ones evaluated with the cross-flow modelling only. Fig. 8 shows the comparison between predictions with and without interaction procedure at the speeds of 6, 8 and 10 knots, considering also the heeling criteria limitations using the $\overline{GZ}$ curve. The maximum forces appears for conditions where thrusters are not in interaction, however interaction occurs for other combinations of τ and β where the equilibrium is still feasible. Fig. 9 shows the contour plots at 8 knots with and without interactions, highlighting how the modelling of the disturbed flow has minor effects on the feasible region of the equilibrium, without changing the maximum values.

4. Proposed general framework

A calculation framework could describe the process needed to determine initial escort characteristics. Follow a precise prediction method allows obtaining the maximum steering and braking forces the unit can deliver in different conditions, potentially starting from few inputs. The process needed to evaluate the escort characteristics implies the resolution of Eqs. (1), (2) and (3) adopting the enhanced equilibrium resolution (11) described in the previous section. The method could suit both initial prediction and advanced design stage ones, just changing the nature of the input provided to the framework; however, the present work deals with preliminary design stage only. The problem resolution requires providing the following inputs:

- position and size of the thrusters;
- position of the towline application point;
- $\overline{GM}$ value or the righting lever curve;
- operational speed;
- hydrodynamic forces.

End users can readily provide the geometrical inputs and the thruster dimensions. However, the determination of hydrodynamic forces and the righting lever curve requires a simplified model for initial design stage application, when more advanced high-fidelity calculations are not at disposal for similar units. Concerning the righting lever curve, the application of the metacentric approximation is a valuable option, as discussed in the previous sections. The modelling of the hydrodynamic forces is more complex and needs a dedicated analysis.

4.1. Hydrodynamic forces

The evaluation of hydrodynamic forces on escort tugs is not an easy task. The nature of the escort operation implies that the tug maintains a speed between 6 and 8 knots, keeping a consistently high drift angle. Such mutual position between hull and incoming flow generates not only a force in the flow direction but also in the perpendicular one. It is usual for escort tugs to define the forces in a flow-oriented reference system, naming the components as lift L_H and drag D_H. Lift and drag derive from tug fixed force components according to the following relationships valid for the adopted reference system:

$$L_H(\beta) = -F_{H_x}(\beta)\sin\beta + F_{H_y}(\beta)\cos\beta \tag{17}$$

$$D_H(\beta) = F_{H_x}(\beta)\cos\beta + F_{H_y}(\beta)\sin\beta \tag{18}$$

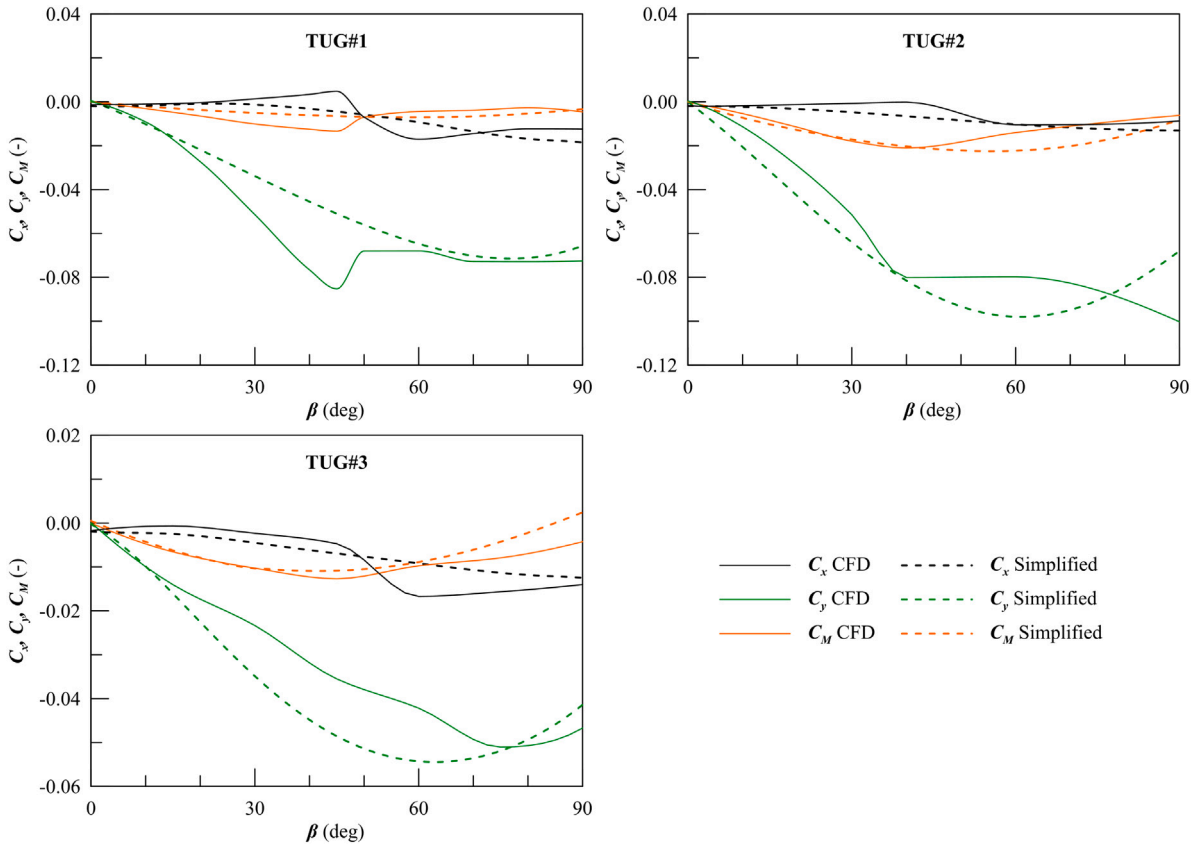

Fig. 10. Non dimensional hydrodynamic force coefficients for the 3 sample escort tugs according to CFD calculations and simplified model.

As hydrodynamic forces are applied to the hull centre of pressure, the application point changes with drift and speed. Thus, there is a momentum respect to tug midship (point O), used as reference for the equilibrium resolution.

The forces can be determined according to different methods. Besides model tests (Sturmhöfel and Bartels, 1993; Molyneux and Woclawek, 2000; Yastreba, 2018), high fidelity tools like CFD can be applied (Molyneux and Bose, 2008; Smoker et al., 2016b; Piaggio et al., 2020). Alternatively, especially for initial predictions, simplified models can be used to reduce the computational effort while keeping a sufficiently accurate estimate of the total forces (Bucci et al., 2016; Yastreba, 2018) for a preliminary escort capability estimation. Between the models there are methods studied for specific escort tug typologies and others, derived from general ship forms, that could apply to more tug types, so giving higher flexibility for the application in an initial design framework.

The flow around a tug advancing with a drift angle β is significantly influenced by viscous effects. Increasing the drift, the occurrence of separation effects increases too, making the viscous modelling critical. However, considering a stationary drift motion in absence of coupling with sinkage and trim, the hydrodynamic forces can be approximated with hydrodynamic derivatives. Considering the lateral and longitudinal velocity components, the forces can be expressed as follows:

$$F_{H_x} = \frac{1}{2}\rho L_{PP}^2 \left(X'_{uu} u|u| + X'_{vv} v^2\right) \tag{19}$$

$$F_{H_y} = \frac{1}{2}\rho L_{PP}^2 \left(Y'_{v} uv + Y'_{vv} v|v|\right) \tag{20}$$

$$M_{H_z} = \frac{1}{2}\rho L_{PP}^3 \left(N'_{v} uv + N'_{vv} v|v| + N'_{vvv} v^3\right) \tag{21}$$

where u and v are the velocity components in x and y directions. Empirical formulations allows to determine hydrodynamic derivatives as a function of few hull geometric parameters. In this study, the following formulations have been used (Ankudinov, 1985; Lee and Shin, 1998):

$$X'_{vv} = \frac{T}{L_{PP}}\left(1.15\frac{C_B B}{L_{PP}} - 0.18\right) \tag{22}$$

$$Y'_{v} = -\pi\left(\frac{T}{L_{PP}}\right)^2 \left[0.25\left(\frac{C_B B}{T}\right)^2 - 1.5\frac{C_B B}{T} + 3.45\right] \tag{23}$$

$$Y'_{vv} = \frac{T}{L_{PP}}\left[0.016\left(\frac{B}{T}\right)^2 - 0.27\frac{B}{T} + 0.0045\frac{L_{PP}}{T} + 1.1\right] \tag{24}$$

$$N'_{v} = -\pi\left(\frac{T}{L_{PP}}\right)^2 \tag{25}$$

$$N'_{vv} = -0.75 N'_{v} \tag{26}$$

$$N'_{vvv} = 0.0348 - 0.5283\left(1 - C_B\right)\frac{T}{B} \tag{27}$$

The pure longitudinal therm of F_{H_x} can be derived from vessel resistance R_T, easily determinable by empirical methods during early design stages (Holtrop, 1984).

The method is similar to the one proposed by Aydin et al. (2018), where the empirical model gave comparable results with CFD calculations on a tractor tug. However, comparison relates L_H and D_H forces only, so according to Eqs. (17) and (18), to F_{H_x} and F_{H_y} only. In the present work the formulation for M_{H_z} has been changed, adding the higher order derivative N'_{vvv}.

Provide a modelling for the hydrodynamic forces acting on the hull is not sufficient for all escort tug. As highlighted in Section 2.1, tractor tugs are characterised by the presence of a large skeg at stern. In such a case, a model has to be given for the evaluation of the hydrodynamic forces due to the appendages. Here a model based on the simplified method (Whickler and Fehlner, 1958) allows determining the skeg contributions in terms of lift and drag force. The lift coefficient has the

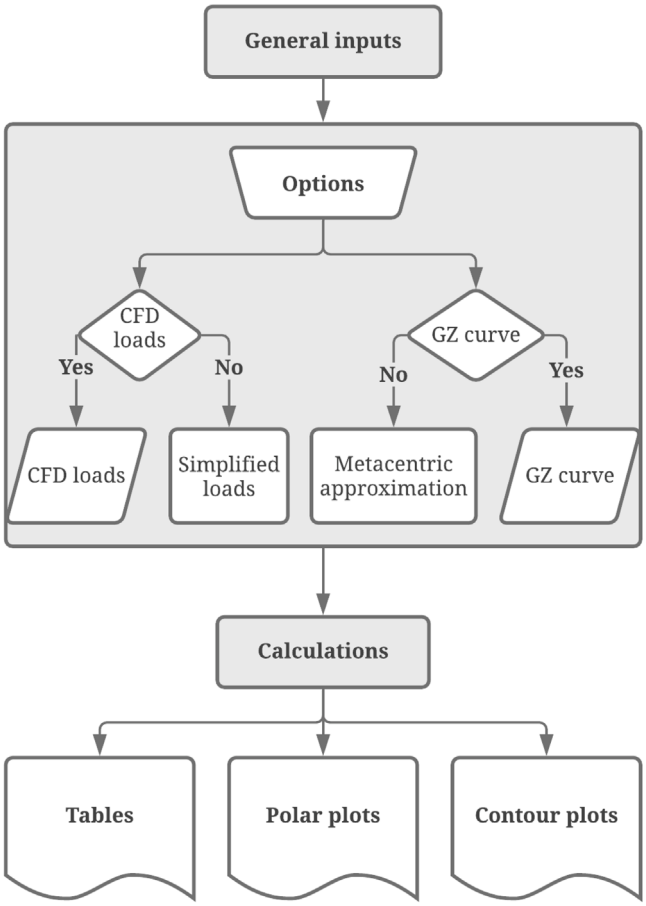

Fig. 11. Workflow for escort tug capability calculations.

following formulation:

$$C_{L_{skeg}} = \frac{\partial C_{Lskeg}}{\partial \beta}\beta + \frac{C_{Dc}}{AR_e}\beta^2 \tag{28}$$

with:

$$\frac{\partial C_{Lskeg}}{\partial \beta} = \frac{1.8\pi AR_e}{1.8 + \cos\Lambda\sqrt{\frac{AR_e^2}{\cos^4\Lambda} + 4}} \tag{29}$$

$$AR_e = \frac{2b^2}{A_L} \tag{30}$$

$$C_{Dc} = 0.1 + 1.6\lambda \tag{31}$$

where A_L is the skeg lateral area, b is the span, Λ the sweep of quarter-chord line and λ is the skeg taper ratio. The drag coefficient derives directly from Eq. (28):

$$C_{D_{skeg}} = 0.0065 + \frac{C_{L_{skeg}}^2}{0.9\pi AR_e} \tag{32}$$

Fig. 10 shows the comparison between the non dimensional hydrodynamic loads calculated with CFD and those obtained with the simplified methods for *TUG#1*, *TUG#2* and *TUG#3*. The non dimensional coefficients have the following formulations:

$$C_x = \frac{F_{H_x}}{\frac{1}{2}\rho L_{PP}^2 V_s^2} \tag{33}$$

$$C_y = \frac{F_{H_y}}{\frac{1}{2}\rho L_{PP}^2 V_s^2} \tag{34}$$

$$C_M = \frac{M_{H_z}}{\frac{1}{2}\rho L_{PP}^3 V_s^2} \tag{35}$$

Analysing the obtained data, it appears that the simplified model is not capable to proper reproduce the CFD-derived loads. This is particularly evident for *TUG#1*, where the peaks around 45° are not captured. Generally, the shape of the C_x and C_y is not well reproduced in the range between $20° < \beta < 70°$, while the C_M is not well reproduced above $\beta > 40°$. On the other end, the simplified method generally captures the magnitude of the coefficients. The adoption of simplified method is therefore suggested only for preliminary predictions, in such a way to have a first starting point for the design of the unit, but not for the final assessment of escort capability of an existing tug. In case CFD loads or model test are available, they will increase the accuracy of the predicted forces.

These differences are influencing the prediction of tug escort capability. The impact will be analysed in the following framework application section.

4.2. Framework workflow

The adoption of an advanced equilibrium resolution method including thruster modelling and heeling limitations allows to estimate the initial capability of different tug types with high flexibility. Moreover, having proposed a simplified model for the hydrodynamic loads calculation and for the righting arm curve approximations, it is then possible providing a calculation framework that needs few inputs to be executed in an initial design stage. To give more flexibility and reliability to the process, the simplified model can be substituted by more complex formulations or by CFD or experimental loads if they are available, as the equilibrium resolution process is independent from the input source.

The process follows the following steps:

- *Input preparation*: in this preliminary step, the general particulars of the tug and of the escort operation are declared. Main dimensions of the tug are provided, giving indications on thrusters position and size together with escort speeds and towing line position. Also the stability criteria can be set.
- *Option selection*: it is possible to select the method to evaluate hydrodynamic loads and righting lever curve. For the simplified method, the additional input required by the process described in the previous section.
- *Calculations*: the equilibrium resolution is performed for a given set of β and τ at each escort speed of interest, finding the maximum towing force F_T for all combinations.
- *Output visualisation*: calculation outputs can be visualised in different forms:
  - polar representation of F_T as a function of τ;
  - contour plot of F_T as a function of β and τ;
  - tables reporting maximum towing, steering and braking force and respective combinations of β and τ.

Fig. 11 provides a schematic overview of the framework workflow for the escort tug capability predictions. Therefore the following set of inputs is needed in case simplified methods are selected:

- *Tug geometry*: L_{PP}, B, T, C_B, $\overline{GM}$.
- *Tug thrusters*: x_{P_i}, y_{P_i}, z_{P_i}, D_i, F_{Pmax_i}.
- *Towline details*: x_T, y_T, z_T.
- *Skeg details (if present)*: Λ, λ, AL_s, b, x_s.
- *Operation details*: V_S, R_T.

Therefore, considering an ASD tug, 21 input values are needed, for a Tractor tug with a skeg 25 inputs and for a Rotor tug 26 input values. If $\overline{GZ}$ curve and hydrodynamic forces from CFD or model tests are available, the input amount reduces.

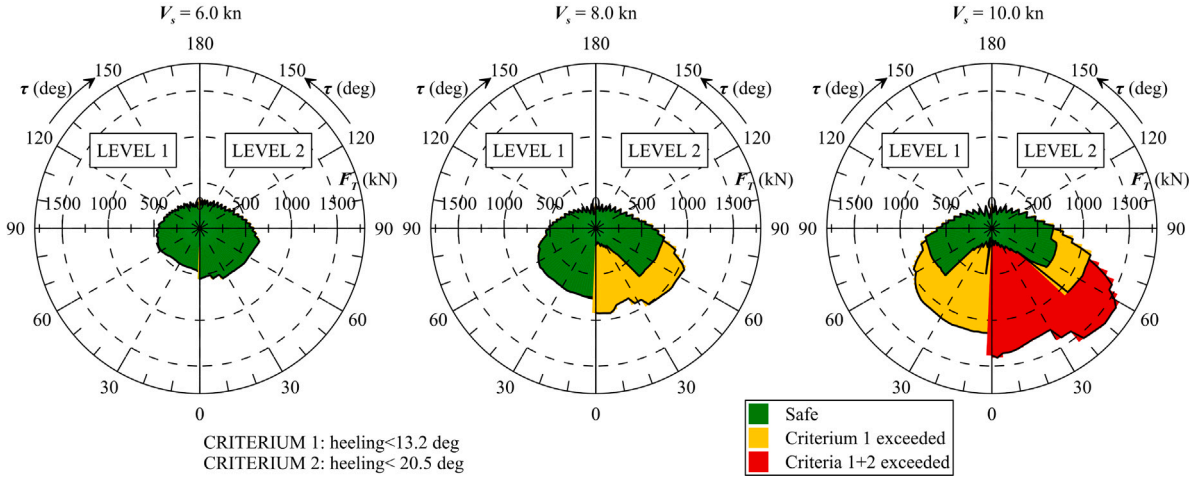

(a) Polar Operability plots with heeling constraints (METHOD 1).

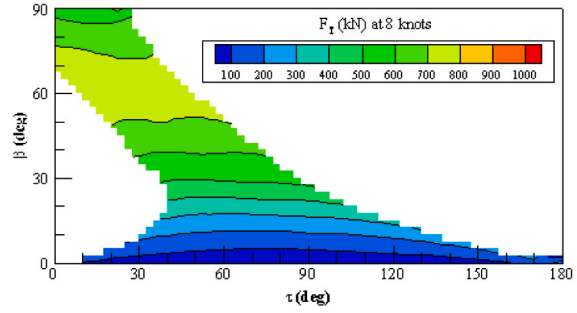

(b) Contour plots of towing force F_T for safe operating conditions at 8 knots, simplified regression loads (METHOD 1-L1).

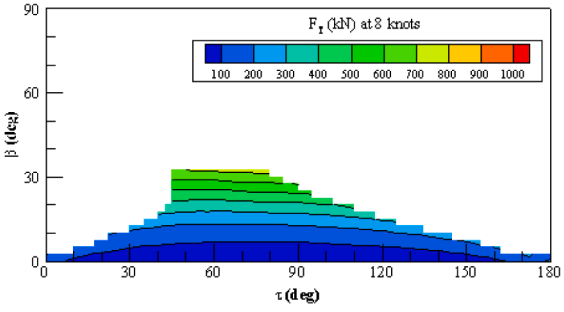

(c) Contour plots of towing force F_T for safe operating conditions at 8 knots, CFD loads (METHOD 1-L2).

Fig. 12. Escort operability for *TUG#1*, comparing the effect of hydrodynamic forces predicted by CFD and simplified formulas.

Table 3
Thrusters and towline positions for the reference tugs.

			TUG#1	*TUG#2*	*TUG#3*
Thruster 1	x_{P_1}	(m)	−9.5	−10.9	−10.1
	y_{P_1}	(m)	−2.5	−2.5	−3.1
	z_{P_1}	(m)	5.0	1.95	5.4
	D_{P_1}	(m)	1.8	2.0	2.2
	$F_{P_{1max}}$	(kN)	175.5	225.4	279.5
Thruster 2	x_{P_2}	(m)	−9.5	−10.9	−10.1
	y_{P_2}	(m)	2.5	2.5	3.1
	z_{P_2}	(m)	5.0	1.95	5.4
	D_{P_2}	(m)	1.8	2.0	2.2
	$F_{P_{2max}}$	(kN)	175.5	225.4	279.5
Thruster 3	x_{P_3}	(m)	–	–	11.2
	y_{P_3}	(m)	–	–	0.0
	z_{P_3}	(m)	–	–	5.2
	D_{P_3}	(m)	–	–	2.2
	$F_{P_{3max}}$	(kN)	–	–	279.5
Towline	x_T	(m)	11.3	9.9	7.5
	y_T	(m)	0.0	0.0	0.0
	z_T	(m)	−4.80	−4.05	−4.85

5. Framework application

In the present section, the proposed general framework is applied to the three sample escort tugs to determine the escort characteristics of the units. Table 3 reports the additional information on thrusters and towing line positions necessary to perform the equilibrium calculations on the units in compliance with reference system of Fig. 1.

The process is capable of also using hydrodynamic loads from external calculations. Therefore, the investigation goes through both the regression formulations and CFD-derived loads, comparing the obtained results. Both the calculation sets apply the metacentric approximation for the righting lever curve $\overline{GZ}$ since the effect of its adoption on escort capability for safe operations is negligible, as already discussed in previous sections.

All the calculations cover a range of β going from 0° to 90° and τ from 0° to 180°. The considered escort speeds are 6, 8 and 10 knots.

The calculation options available in the framework using the metacentric approximation can be summarised as follows:

- *METHOD 0*: this option adopts the metacentric approximation for the righting arm, and the powered indirect mode for the equilibrium resolution, thus reflecting a state-of-art and officially accepted method to predict initial escort performances for a tug.
- *METHOD 1*: this method is using the advanced equilibrium resolution based on the thrust allocation algorithm, considering propeller interactions. The transversal equilibrium is evaluated according to the metacentric approximation.

Both methods can be applied with two different options for the hydrodynamic loads, providing two different levels of accuracy for the preliminary design stage predictions:

- *LEVEL 1* (L1): the hydrodynamic coefficients are derived from empirical regression formulations (19), (20) and (21).
- *LEVEL 2* (L2): the hydrodynamic coefficients are predicted by CFD calculations.

For reader perusal, the prediction results presented in the following sections refer to *METHOD 0-L1*, *METHOD 1-L1* and *METHOD 1-L2*.

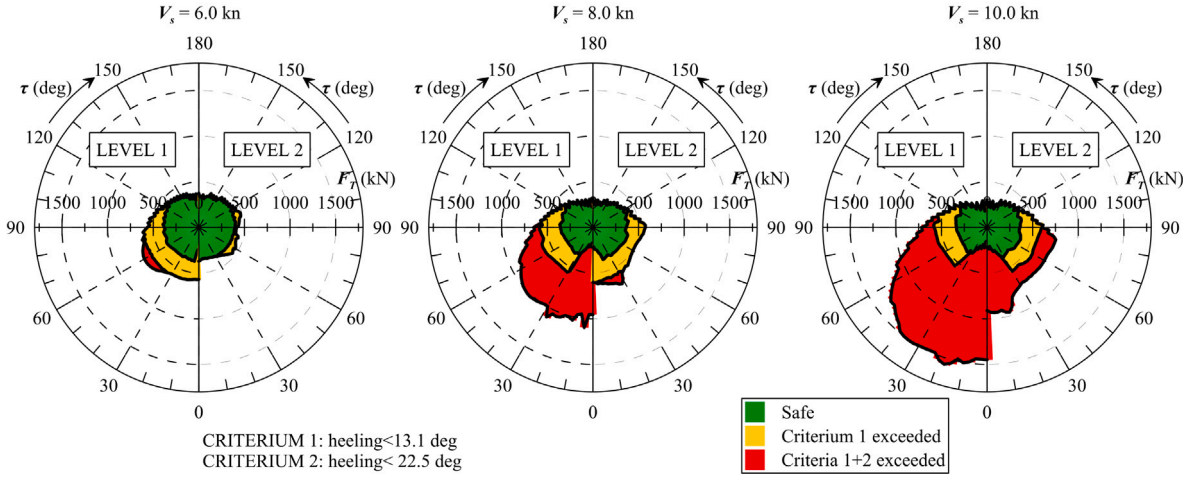

(a) Polar operability plots with heeling constraints (METHOD 1).

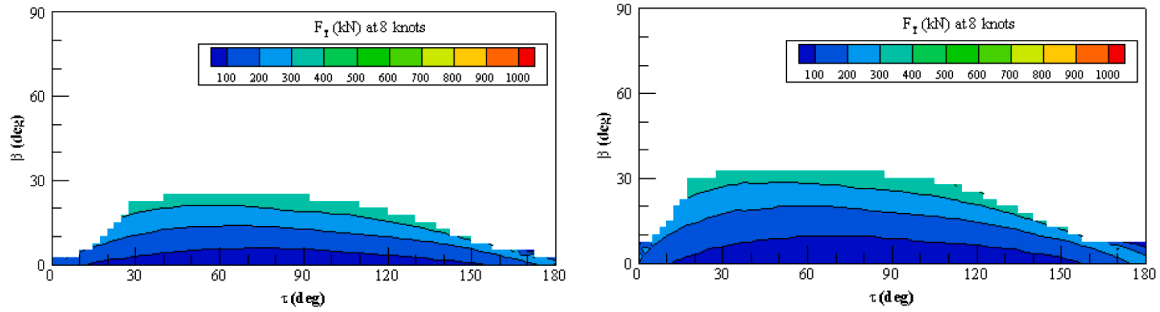

(b) Contour plots of towing force F_T for safe operating conditions at 8 knots, simplified regression loads (METHOD 1-L1).

(c) Contour plots of towing force F_T for safe operating conditions at 8 knots, CFD loads (METHOD 1-L2).

Fig. 13. Escort operability for *TUG#2*, comparing the effect of hydrodynamic forces predicted by CFD and simplified formulas.

In the following sections the results of the calculation framework are reported and discussed on each sample tug with the aid of plots and tables, using the described nomenclature within the calculation methods. The tables results report not only the maximum towing force F_T, but also the conditions where the steering force F_S and the braking force F_B reach their respective maxima. A comparison with the conventional powered-indirect mode for the equilibrium resolution (METHOD 0-L1) highlights the benefits that can be obtained by METHOD 1 by using the enhanced equilibrium resolution implemented in the framework.

5.1. TUG#1 analysis

TUG#1 is an example of tractor tug used as reference in the previous discussion on righting lever curve and thruster interaction. As shown in Fig. 3, the tug has a skeg in the aft, therefore it is necessary to provide its geometric informations to apply the regression method for hydrodynamic loads evaluation. In the specific the values are as follows: b= 3.2 m, x_s= 12.4 m, AL_s= 12.8 m^2, Λ= 0.09 rad, λ= 0.9.

Fig. 12(a) shows the polar plots at the speeds of 6, 8 and 10 knots obtained from the calculations performed with METHOD 1-L1 and METHOD 1-L2, thus highlighting the effect of the empirical regressions and CFD-derived hydrodynamic loads on tug operability. It can be observed that the maximum towing force F_T envelope changes with the hydrodynamic loads source, as it was advisable comparing the coefficients (see Fig. 10). Not only the maximum towing force envelope changes but also the envelopes associated to the safety criteria. For 6 knots, all the operations are performed in safety zone. At 8 knots, the METHOD 1-L1 detects only safe equilibrium conditions, while applying METHOD 1-L2 one criterium is exceeded in some conditions, reducing the safe operation envelope. At 10 knots, applying METHOD 1-L1 only one safety criterium is exceeded, while METHOD 1-L2 detects also areas where both the criteria are not satisfied.

The impact of the environmental loads is visible also in the feasible area of operations, not only in the maximum values. Figs. 12(b) and 12(c) show as an explicative example the towing force contour plot in safe conditions at the speed of 8 knots using METHOD 1-L1 and METHOD 1-L2, respectively. The two contours identify two different feasible areas of operations. The results from METHOD 1-L2 show a smaller region of feasibility, predicting safe operations up to a β angle around 33°. Using METHOD 1-L1, the feasible area increases finding feasible safe solution through the whole β range.

Concerning the forces values delivered by the tug, Table 4 provides a resume of the maximum values for the towing force F_T, the steering force F_S and the braking force F_B together with the associated τ, β and ϕ angles. For 6 knots, the predicted maximum forces with METHOD 1-L1 are 20% to 30% lower than the ones resulting from METHOD 1-L2. For other speeds the differences are around 10%–12%. The same table reports also the forces obtained by applying METHOD 0-L1. The results, compared to the enhanced resolution method with the same hydrodynamic loads modelling (METHOD 1-L1), highlight that the simplified resolution detects lower escort forces for 6 an 8 knots, with discrepancies between 25% and 50% in the maximum values. Moreover, METHOD 0-L1 in not capable to predict the maximum force in safe conditions for the speed of 10 knots.

5.2. TUG#2 analysis

TUG#2 is an example of ASD tug. The dimensions of the tug are smaller compared to *TUG#1*; however, the size of the thrusters is higher (see Table 1).

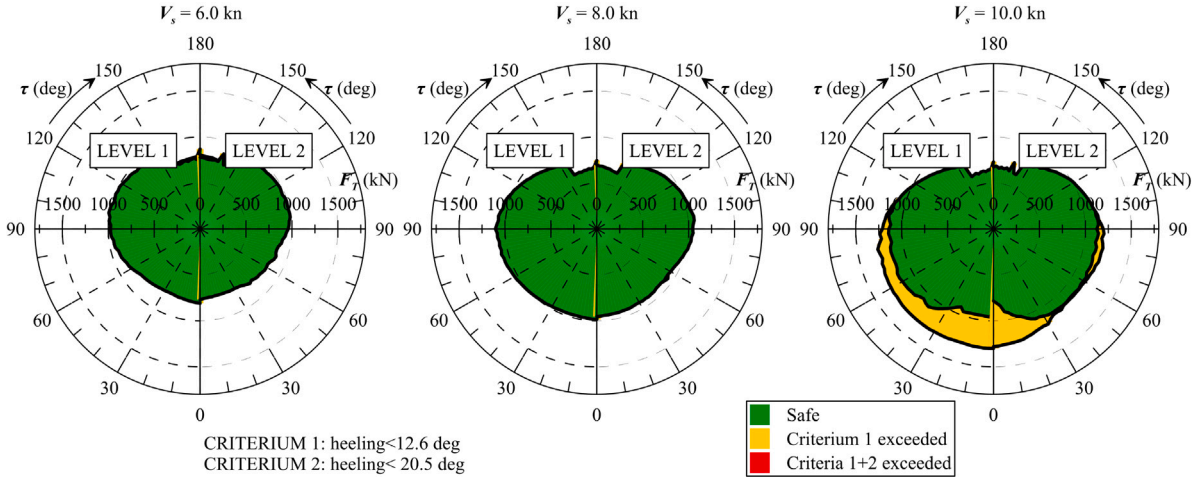

(a) Polar operability plots with heeling constraints (METHOD 1).

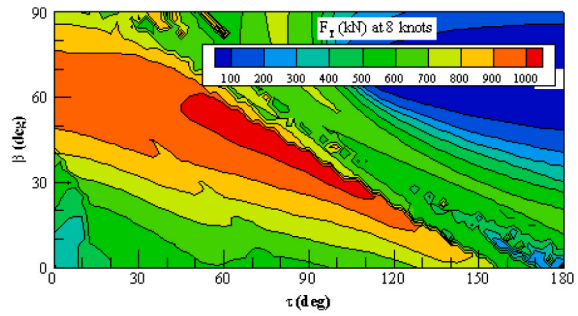

(b) Contour plots of towing force F_T for safe operating conditions at 8 knots, simplified regression loads (METHOD 1-L1).

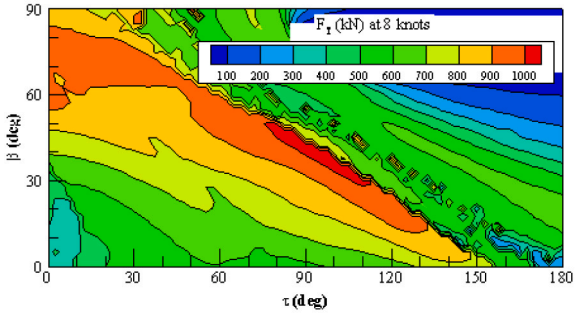

(c) Contour plots of towing force F_T for safe operating conditions at 8 knots, CFD loads (METHOD 1-L2).

Fig. 14. Escort operability for *TUG#3*, comparing the effect of hydrodynamic forces predicted by CFD and simplified formulas.

Table 4
Escort operability in safe conditions for *TUG#1*.

Quantity			METHOD 1-L2			METHOD 1-L1			METHOD 0-L1		
			6 knots	8 knots	10 knots	6 knots	8 knots	10 knots	6 knots	8 knots	10 knots
Max. towing force	$F_{T_{max}}$	(kN)	650.0	745.0	735.0	490.0	750.0	730.0	434.6	609.0	881.3
Towline angle	τ	(deg)	77.5	80.0	65.0	65.0	0.0	27.5	102.3	122.6	136.6
Drift angle	β	(deg)	45.0	32.5	25.0	62.5	67.5	82.5	57.0	58.0	59.0
Heeling angle	ϕ	(deg)	10.7	12.3	12.3	7.7	12.3	12.1	5.6	10.1	15.8
Max. braking force	$F_{B_{max}}$	(kN)	545.0	495.0	415.8	475.0	750.0	509.1	341.9	300.5	316.6
Towline angle	τ	(deg)	0.0	45.0	55.0	0.0	0.0	45.0	0.0	0.0	0.0
Drift angle	β	(deg)	52.5	22.0	25.0	52.5	67.5	27.5	0.0	0.0	0.0
Heeling angle	ϕ	(deg)	8.8	11.8	12.3	7.4	12.3	12.0	0.0	0.0	0.0
Max. steering force	$F_{S_{max}}$	(kN)	649.2	733.7	700.3	472.7	625.4	783.8	430.4	556.0	725.0
Towline angle	τ	(deg)	77.5	80.0	75.0	80.0	65.0	27.5	94.9	107.0	115.1
Drift angle	β	(deg)	45.0	32.5	25.0	50.0	47.5	82.5	51.0	46.0	43.0
Heeling angle	ϕ	(deg)	10.7	12.3	12.3	7.4	11.4	12.3	5.5	9.4	14.4

Fig. 13(a) shows the polar plots at the speeds of 6, 8 and 10 knots obtained from the calculations performed with METHOD 1-L1 and METHOD 1-L2. The different nature of the hull-form, compared to the tractor tug, generates a different shape for the CFD-derived hydrodynamic loads (METHOD 1-L2). Such a difference impacts the polar envelopes, which, contrarily to *TUG#1* are wider for the simplified loads modelling (METHOD 1-L1), without taking into account the heeling constraints. Considering the safe region, the values obtained with the two hydrodynamic loads options are close with each other, having differences under 10%, as it can be observed with data in Table 5. The two contour plots in Figs. 13(b) and 13(c) for the reference speed of 8 knots confirm the small differences also for the feasible safe operation region, compared to the previous case.

Both METHOD 1-L1 and METHOD 1-L2 detect a lower braking force F_B compared to METHOD 0-L1. This is due to the propulsor modelling, not present in METHOD 0-L1. For this tug, METHOD 0-L1 is not capable to detect safe equilibrium conditions for all the three tested speeds.

5.3. *TUG#3 analysis*

TUG#3 is an example of rotor tug. As already mentioned, this vessel typology is quite different from the others as it has three steerable thrusters (Table 3).

Fig. 14(a) shows the polar plots at the speeds of 6, 8 and 10 knots obtained from the calculations performed with METHOD 1-L1 and METHOD 1-L2. It can be observed that the two methods, differing only for the loads modelling, provide similar envelops for all the three tested

Table 5
Escort operability in safe conditions for *TUG#2*.

Quantity			METHOD 1-L2			METHOD 1-L1			METHOD 0-L1		
			6 knots	8 knots	10 knots	6 knots	8 knots	10 knots	6 knots	8 knots	10 knots
Max. towing force	$F_{T_{max}}$	(kN)	420.0	410.0	400.0	430.0	400.0	400.0	463.3	522.2	646.8
Towline angle	τ	(deg)	122.5	122.5	120.0	135.0	130.0	132.5	74.6	98.7	119.1
Drift angle	β	(deg)	32.5	25.0	20.0	20.0	17.5	12.5	49.0	54.0	56.0
Heeling angle	ϕ	(deg)	13.1	13.1	13.1	12.5	13.0	13.1	14.9	28.14	32.1
Max. braking force	$F_{B_{max}}$	(kN)	370.0	352.9	328.2	287.3	234.6	239.6	444.8	435.8	421.4
Towline angle	τ	(deg)	0.0	17.5	27.5	7.5	27.5	30.0	0.0	0.0	0.0
Drift angle	β	(deg)	37.5	30.0	22.5	32.5	22.5	12.5	0.0	0.0	0.0
Heeling angle	ϕ	(deg)	12.6	13.0	13.2	13.0	13.2	11.3	0.0	0.0	0.0
Max. steering force	$F_{S_{max}}$	(kN)	401.5	388.9	375.9	380.8	375.9	378.6	459.5	519.8	608.0
Towline angle	τ	(deg)	97.5	100.0	102.5	62.5	77.5	77.5	86.0	93.1	102.0
Drift angle	β	(deg)	42.5	30.0	22.5	40.0	22.5	17.5	59.0	50.0	44.0
Heeling angle	ϕ	(deg)	13.1	13.2	13.0	13.1	13.1	13.1	15.5	27.0	30.7

Table 6
Escort operability in safe conditions for *TUG#3*.

Quantity			METHOD 1-L2			METHOD 1-L1			METHOD 0-L1		
			6 knots	8 knots	10 knots	6 knots	8 knots	10 knots	6 knots	8 knots	10 knots
Max. towing force	$F_{T_{max}}$	(kN)	990.0	1065.0	1175.0	1010.0	1105.0	1175.0	830.6	840.5	892.7
Towline angle	τ	(deg)	100.0	95.0	90.0	100.0	90.0	92.5	25.9	53.6	74.5
Drift angle	β	(deg)	42.5	40.0	37.5	40.0	40.0	30.0	18.0	32.0	38.0
Heeling angle	ϕ	(deg)	9.8	11.2	13.1	10.2	12.2	13.1	1.3	3.1	4.9
Max. braking force	$F_{B_{max}}$	(kN)	770.0	955.0	1038.4	810.0	985.0	991.4	829.4	818.0	804.1
Towline angle	τ	(deg)	0.0	0.0	20.0	0.0	0.0	7.5	0.0	0.0	0.0
Drift angle	β	(deg)	55.0	72.5	50.0	55.0	60.0	87.5	0.0	0.0	0.0
Heeling angle	ϕ	(deg)	7.3	11.1	13.1	8.3	12.1	12.9	0.0	0.0	0.0
Max. steering force	$F_{S_{max}}$	(kN)	981.5	1060.9	1175.0	994.7	1105.0	1173.9	766.2	794.6	879.7
Towline angle	τ	(deg)	97.5	95.0	90.0	100.0	90.0	92.5	79.4	79.0	83.4
Drift angle	β	(deg)	45.0	40.0	37.5	40.0	40.0	30.0	66.0	52.0	44.0
Heeling angle	ϕ	(deg)	9.0	11.2	13.1	10.2	12.2	13.1	1.3	2.5	4.7

speeds. In fact, comparing the non-dimensional coefficients in Fig. 10, it is possible to observe that the main difference is in the shape of C_y coefficient only.

Analysing the contour plots for 8 knots reported in Figs. 14(b) and 14(c) it can be observed that the feasible operability range of this escort tug type is wider than all the other units. The mentioned figures report the speed of 8 knots, but the same considerations are valid for the other not reported speeds. Having a look to the results for maximum forces reported in Table 6 confirms that the variations for the safe conditions are in the magnitude of 5% between CFD-derived loads and regression method ones.

The results of METHOD 0-L1 detect maximum forces achievable in a safe condition. However, the values compared with the advanced procedure differ for about 25% with respect to the advanced resolution. The difference for this tug is the highest compared to the other analysed units.

5.4. Final remarks

The framework testing on the three reference tugs highlights that the proposed methodology is flexible for the analysis of escort tug types commonly used for operations. The advanced method for the equilibrium resolution has higher capabilities compared to the standard powered-indirect mode METHOD 0. This was already highlighted in the early procedure development (Mauro, 2021), but the application on a wider range and typology of tugs further stressed it. The possibility to handle more than two thrusters without changing the calculation strategy allows the analysis of particular cases as rotor tugs (*TUG#3*), where the traditional calculation method (*METHOD 0*) merges all thrusters in a single group. On the other hand, the results on sample tugs using different sources for environmental loads shows that the adoption of simplified regression models has a substantial impact on the prediction of tug escort capabilities. Besides a change in the final value of towing forces, also the combinations of β and τ change as well. Therefore the accuracy of the framework is strictly related to the selection of the hydrodynamic loads calculation method. It is then mandatory to consider the simplified method only for really preliminary predictions, when it is necessary to evaluate macroscopic changes in tug dimensions or variations in the thruster layout, using the calculation results for comparative purposes. General regression from literature are far too general to reproduce the hydrodynamic coefficients for escort tugs through a wide range of β angles. However, if higher fidelity hydrodynamic loads are available, the proposed process leads to a more reliable prediction than commonly accepted approaches for preliminary design stage. The application of simplified models for hydrodynamic loads requires dedicated studies to produce empirical regression specific for different escort tug types.

6. Conclusions

The presented work treated diverse issues concerning the performance predictions for escort tugs in the initial design stage to propose a flexible calculation framework suitable for different tug types. Additional features on heeling limitations and thrusters interaction improve an already advanced method developed for the equilibrium resolution (Mauro, 2021). In particular, the addition of the heeling limitations, compliant with classification societies rules, significantly impact the final capability of the escort unit. The calculation method (METHOD 1) allows identifying the maximum towing forces generated in safe mode.

It has been shown that the thruster interactions effects have a low impact on the maximum forces delivered by the tug, which occur when thrusters are not in interactions or are not fully saturated. However, the interaction modelling is influencing the feasible domain of escort operations. It is therefore advisable to consider it during calculations, particularly when tugs with multiple thrusters are investigated

in detail. Moreover, the enhancements here presented do not require additional inputs that are unknown in the initial design stage.

A framework suitable for the initial design stage requires simplified models to evaluate quantities that could be unknown as the hydrodynamic forces and the righting lever curve. For the righting lever curve $\overline{GZ}$ the metacentric approximation has a low impact on the predicted escort capabilities for the tested tugs, showing differences of less than 1% compared to the adoption of the $\overline{GZ}$ curve.

Hydrodynamic forces are the most complex issue as they deal with the specific hull form of the tug and its appendages. The calculation framework adopts a simplified method based on the hydrodynamic derivatives. The comparison of non-dimensional loads shows that the simplified empirical regression model is not capable of exactly reproducing the CFD-derived coefficients. However, the methodology captures the magnitude of the loads coefficients. The differences in hydrodynamic loads reflect in the tug capability predictions. However, even though the maximum capability without heeling limits is much different, the prediction of the safety escort region is more in line with CFD-derived results. Therefore, the simplified method can be used at least to compare different solutions in the initial design stage. A more reliable initial prediction requires the adoption of hydrodynamic force coefficients predicted with CFD or measured during model tests.

The present study highlighted that the advanced methodologies used to solve the equilibrium are capable to handle several escort tug types, giving a significant progress compared to traditional methods. Further studies are needed to identify a proper simplified regression model for the hydrodynamic forces, as an example, using models derived from sets of experiments or validated CFD calculations on different families of tugs. The generalisation of such or other high-fidelity models for hydrodynamic forces will further increase the reliability of the predictions obtained through the implemented framework.

Declaration of competing interest

The authors declare that they have no known competing financial interests or personal relationships that could have appeared to influence the work reported in this paper.

References

Abramovich, G.N., 1960. The Theory Of Turbulent Jets, English MIT Press, Cambridege, Mass..

Allan, R.G., 2006. A proposal for the harmonised international regulations for the design and construction of tugboats. In: International Towage And Salvage Conference. Rotterdam.

Allan, R., Molyneux, D., 2004. Escort tug design alternatives and a comparison of their hydrodynamic performance. Trans. SNAME (112), 191–205.

Ankudinov, V., 1985. Ship manoeuvring simulation model including regimes of slow speeds and large drift angles. In: First International Maritime Simulation Symposium. Munich, Germany.

Arditti, F., Cozijn, H., Van Daalen, E., Tannuri, E.A., 2019. Robust thrust allocation algorithm considering hydrodynamic interactions and actuator physical limitations. J. Mar. Sci. Technol. 24 (4), 1057–1070.

Aydin, C., Ünal, U., Karambulut, U., Sariöz, K., 2018. Practical computational procedures for predicting steering and breaking forces on escort tugs. Ocean Eng. (166), 159–171.

Brandner, P., Renilson, M., 1998. Interaction between two closely spaced azimuthing thrusters. J. Ship Res. 42 (1), 15–31.

Bucci, V., Marinò, A., 2016. On the calculation of the forces developed by escort tugs. Annu. Dunarea De Jos Univ. Galati (XI), 61–77.

Bucci, V., Marinó, A., Mauro, F., 2016. Quasi-steady determination of dynamic forces acting on tug during escort operations. In: Proceedings of 3rd International Conference on Maritime Technology and Engineering, MARTECH 2016.

de Jong, J.H., 2007. Ship assist in fully exposed conditions - joint industry project safe tug. Tugnology 2007, Southampton.

ETA, 2015. Guidelines for Harbour Towage Operations. Tech. Rep, European Tugowners Association.

Holtrop, J., 1984. A statistical re-analysis of resistance and propulsion data. Int. Shipbuild. Prog. 31, 272–276.

Hyslop, J., Hass, D., Chandan, D., den Hertog, V., Smoker, B., 2018. The escort issue. Raindrops 17.

Iglesias-Baniela, S., Vinagre-Rios, J., Perez-Canosa, J.M., 2021. Ship handling in unprotected waters: a review of new technologies in escort tugs to improve safety. Appl. Mech. 2, 46–62.

IMO, 2016. MSC.415(97), Amendments to Part B of the International code on Intact stability, 2008 (2008 IS Code). Tech. Rep, International Maritime Organisation, as amended on 25 november 2016.

Lee, H.Y., Shin, S.S., 1998. The prediction of ship's manoeuvring performance in initial design stage. Dev. Mar. Technol. 11, 633–639.

Lehn, E., 1980. Thruster Interaction Effects. Tech. Rep. R-102.80, NSFI.

Mauro, F., 2021. Thruster modelling for escort tug capability predictions. Ocean Eng. 229, 108967.

Mauro, F., Nabergoj, R., 2016. Advantages and disadvantages of thruster allocation procedures in preliminary dynamic positioning predictions. Ocean Eng. 123, 96–102.

Molyneux, D., Bose, N., 2008. Escort tug at large yaw angle: comparison of CFD predictions with experimental data. Int. J. Small Craft Technol. Part B1 (150).

Molyneux, D., Woclawek, P., 2000. Predicting the performance of a tug and a tanker during escort operation using computer simulations and model tests. Trans. SNAME (108), 21–44.

Paulauskas, V., Simutis, M., Placiene, B., Barzdziukas, R., Jonkus, M., Paulauskas, D., 2021. The influence of port tugs on improving the navigational safety of the port. J. Mar. Sci. Eng. 9 (342), 1–20.

Piaggio, B., Villa, D., Viviani, M., 2020. Numerical analysis of escort tug manoeuvrability characteristics. Appl. Ocean Res. 97, 102075.

Piaggio, B., Viviani, M., Martelli, M., Figari, M., 2019. Z-drive Escort tug manoeuvrability model and simulation. Ocean Eng. 191, 106461.

Prpić-Oršić, J., Valčić, M., 2020. Derivative free optimal thrust allocation in ship dynamic positioning based on direct search algorithms. TransNav 14 (2), 309–314.

Quadvlieg, F., Kaul, D., 2006. Development of a calculation program for escort forces and stern drive tug boats. In: 19th International Tug And Salvage Convention And Exhibition.

Sas, F., Timmers, R., Gallin, C., 1993. Simulation of the effective pull forces produced by tugs. In: RINA International Conference On Escort Tug Design, Construction And Handling. (7).

Smoker, B., 2012. Escort Tug Performance Prediction: a CFD Method. (Master's thesis). University of Victoria.

Smoker, B., Stockdill, B., Oshkai, P., 2016a. Escort tug performance prediction using computational fluid dynamics. J. Ship Res. 60, 61–77.

Smoker, B., Stockdill, B., Oshkai, P., 2016b. Escort tug performance prediction using computational fluid dynamics. J. Ship Res. (60), 61–77.

Sturmhöfel, U., Bartels, J., 1993. Basic requirements for safe escort vessels – theoretical considerations and model measurements. In: RINA International Conference On Escort Tug Design, Construction And Handling.

Tackinaci, A., Erginer, K., 2017. A simple two-dimensional method for predicting escort performance of a tug having azimuth stern drives. In: Pilotage / Towage Services And Technology Congress.

Whickler, L.F., Fehlner, L.F., 1958. Free Stream Characteristics of a Famiy of Low Aspect Ratio, All Movable Control Surface for Application to Ship Design. Tech. Rep. 933, David Taylor Model Basin.

Yastreba, O.P., 2018. Method for the determination of escort tugs main dimensions and charachteristics at conceptual design stage. Shipbuil. Mar. Infrastructures 2 (10), 27–35.